SCIENCE CHINA
Physics, Mechanics & Astronomy

•Article•

December 2021 Vol. 64 No. 12: 127411
https://doi.org/10.1007/s11433-021-1804-7

Surface morphology and electronic structure in stoichiometric superconductor $CaKFe_4As_4$ probed by scanning tunneling microscopy/spectroscopy

Xiaodong Yu[1,2], Zhongxu Wei[1,2*], Zhanyi Zhao[1,2], Tao Xie[1,2], Chang Liu[1,2], Ge He[3], Qihong Chen[1,2], Lei Shan[4], Huiqian Luo[1,5], Qing Huan[1,5], Jie Yuan[1,5], and Kui Jin[1,2,5]

[1] *Beijing National Laboratory for Condensed Matter Physics, Institute of Physics, Chinese Academy of Sciences, Beijing 100190, China;*
[2] *School of Physical Sciences, University of Chinese Academy of Sciences, Beijing 100049, China;*
[3] *Walther Meissner Institute, Bayerische Akademie der Wissenschaften, Garching 85748, Germany;*
[4] *Key Laboratory of Structure and Functional Regulation of Hybrid Materials of Ministry of Education, Institutes of Physical Science and Information Technology, Anhui University, Hefei 230601, China;*
[5] *Songshan Lake Materials Laboratory, Dongguan 523808, China*

Received August 2, 2021; accepted October 28, 2021; published online November 4, 2021

$CaKFe_4As_4$ is a new-type superconductor with a relatively high transition temperature of 35 K among stoichiometric iron-based superconductors. Based on scanning tunneling microscopy/spectroscopy, the surface morphology and electronic structure of $CaKFe_4As_4$ single crystal were systematically investigated. The cleaved $CaKFe_4As_4$ showed various morphologies, such as atomically resolved 1×1, 1×2, and $\sqrt{2} \times \sqrt{2}$ lattices. By analyzing the geometrical correlations of these morphologies, the 1×1 and 1×2 lattices were identified as the original and reconstructed As layers, respectively, whereas the $\sqrt{2} \times \sqrt{2}$ lattice was distinguished as the reconstructed alkaline-earth-metal or alkali-metal layer. The superconducting energy gap of 7.3 meV and bosonic mode of 12.7 meV were resolved in the scanning tunneling spectra. In addition, the superconducting energy gaps measured on different terminations were identical and consistent with the values obtained by bulk-sensitive techniques, indicating that the electronic structures of $CaKFe_4As_4$ were insensitive to the surface reconstructions. Our study clarifies the relationships between complex surface reconstructions and surface terminations and preliminarily presents that there is no obvious effect of surface reconstructions on electronic states.

$CaKFe_4As_4$, scanning tunneling microscopy, surface reconstructions, superconductivity

PACS number(s): 68.35.Bs, 68.37.Ef, 74.70.-b

Citation: X. Yu, Z. Wei, Z. Zhao, T. Xie, C. Liu, G. He, Q. Chen, L. Shan, H. Luo, Q. Huan, J. Yuan, and K. Jin, Surface morphology and electronic structure in stoichiometric superconductor $CaKFe_4As_4$ probed by scanning tunneling microscopy/spectroscopy, Sci. China-Phys. Mech. Astron. **64**, 127411 (2021), https://doi.org/10.1007/s11433-021-1804-7

1 Introduction

Scanning tunneling microscopy/spectroscopy (STM/S) is a robust tool for investigating superconducting properties in nanoscale [1-5]. Owing to the clean surface requirement for STM probing, samples generally need to be fabricated *in situ* or cleaved under a high vacuum. For most layered cuprate and iron-based superconductors with charge reservoir intercalation, the cleaved surfaces are not unique, and their electronic structures could differ. For example, two kinds of

*Corresponding author (email: zhongxuwei@iphy.ac.cn)

surface morphologies, 1×2 stripes and 1×1 lattices, are observed in cleaved $Sr_{0.75}K_{0.25}Fe_2As_2$ [6]. The tunneling spectra measured on a surface with stripes have a pair of superconducting coherent peaks, whereas there is no well-defined peak in tunneling spectra taken on 1×1 lattices [6]. In addition, various surface terminations are resolved in both $Ba(Fe,Co)_2As_2$ and $Ba_{0.6}K_{0.4}Fe_2As_2$, and the tunneling spectra show a dependence on terminations [7,8]. For cuprate superconductor $Bi_2Sr_2CaCu_2O_8$, the U-shaped tunneling spectra collected on the CuO_2 layer contrast the V-shaped spectra measured on the BiO surface [9,10], which challenges the *d*-wave pairing scenario in cuprates. Therefore, it is essential to identify different surface terminations and study the termination-dependent electronic structures.

Various surface reconstructions, such as 1×2 and $\sqrt{2}\times\sqrt{2}$ lattices, have been observed by STM in cleaved 122-type iron pnictide compounds. However, the type of cleaved terminations remains controversial. There are two main points about the determination of cleaved terminations held by STM groups [11]. Combined with the crystal structure, some STM groups attribute the 1×2 and $\sqrt{2}\times\sqrt{2}$ lattices to the reconstructions of alkaline-earth-metal (AE) and As layers, respectively [12-14], whereas others argue that the observed surface reconstructions result from the As layer, but half of As atoms are "invisible" to STM [7,11,15,16]. Moreover, low-energy electron diffraction experiments indicate that the AE layer can form either 1×2 lattice [17] or $\sqrt{2}\times\sqrt{2}$ lattice [18,19], and the reconstructed As layer can exhibit $\sqrt{2}\times\sqrt{2}$ lattice [12]. In addition, theoretical calculations identify the $\sqrt{2}\times\sqrt{2}$ structure as the reconstruction of the AE layer [20]. Overall, two crucial questions need to be clarified in 122-type compounds. (1) What are the relationships between surface morphologies and surface terminations? (2) Will electronic structures, such as superconducting gaps, be significantly modified by surface reconstructions?

$CaKFe_4As_4$ is a suitable candidate for clarifying these questions. As shown in Figure 1(a), the crystal structure of $CaKFe_4As_4$ can be regarded as an alternating stack of alkali-metal (A) and AE layers across As-Fe-As layers [21,22], which is similar to the structure of 122-type compounds [23,24]. Therefore, the cleaved terminations of $CaKFe_4As_4$ and 122-type compounds are expected to have the same geometric structures. An obvious difference between $CaKFe_4As_4$ and 122-type compounds is that the superconductivity of the latter requires the introduction of hole or electron dopants [25-27]. Since disorder effects induced by the random distribution of dopants are difficult to avoid in 122-type compounds [6,28], the stoichiometric superconductor $CaKFe_4As_4$ is more suitable for studying the impact of surface reconstructions on electronic structures.

In this study, we perform systematic measurements of STM/S on $CaKFe_4As_4$ single crystals. Several surface morphologies, such as 1×1, 1×2, and $\sqrt{2}\times\sqrt{2}$ lattices, are clearly resolved. Based on the geometrical relationships of these morphologies, we conclude that the 1×1 and 1×2 lattices correspond to the original and reconstructed As layers, respectively, whereas the $\sqrt{2}\times\sqrt{2}$ lattice originates from the reconstructed AE/A layers. The tunneling spectra collected on different reconstructed surfaces have quite similar characteristics, such as the superconducting energy gap and bosonic mode. In addition, the superconducting gap measured by our STS experiments is similar to the results of bulk-sensitive techniques, such as tunnel-diode resonator [29], polarization-resolved Raman spectroscopy [30], muon spin rotation and relaxation [31], nitrogen-vacancy centers magnetometry [32], and optical conductivity [33]. Therefore, there is no obvious effect of surface reconstructions on electronic structures of $CaKFe_4As_4$ single crystals.

2 Experimental details

The $CaKFe_4As_4$ single crystals used in this study are prepared via the self-flux method [21,22,34]. Figure 1(b) and (c) show the transport and magnetization measurements of $CaKFe_4As_4$. The high zero-resistance critical transition temperature T_c of 35 K with sharp superconducting transition indicated that the samples were of high quality. The experiments of surface morphologies and tunneling spectra were performed in a home-built STM [35]. $CaKFe_4As_4$ single crystals were first precooled to ~120 K in 2×10^{-10} Torr a high vacuum and then cleaved *in situ*. Commercial Pt/Ir tips (Unisoku Co., Ltd.) were calibrated on a clean Au(111) surface before performing STM/S experiments. A constant-current mode was used to obtain topographic images, and the bias voltage was applied to the sample. The tunneling spectra were measured using a standard lock-in technique with a 0.2 mV modulation voltage at 973 Hz. The STM/S experiments were performed at 6 K.

3 Results and discussion

Figure 2(a) depicts a typical topographic image of $CaKFe_4As_4$. The surface morphology can be divided into two regions, labeled Region-I and Region-II. Region-II is full of separated stripes. Figure 2(b) shows the zoom-in morphology of Region-II. The averaged distance between adjacent stripes was ~7.8 Å, which was approximately two times the in-plane lattice constant of $CaKFe_4As_4$ [21]. Therefore, the stripes observed were probably the so-called 1×2 reconstructions observed in 122-type compounds. In addition, as shown by the green and yellow lines in Figure 2(b), stripes could rotate 90° and possess phase shifts of half a unit, which agreed with

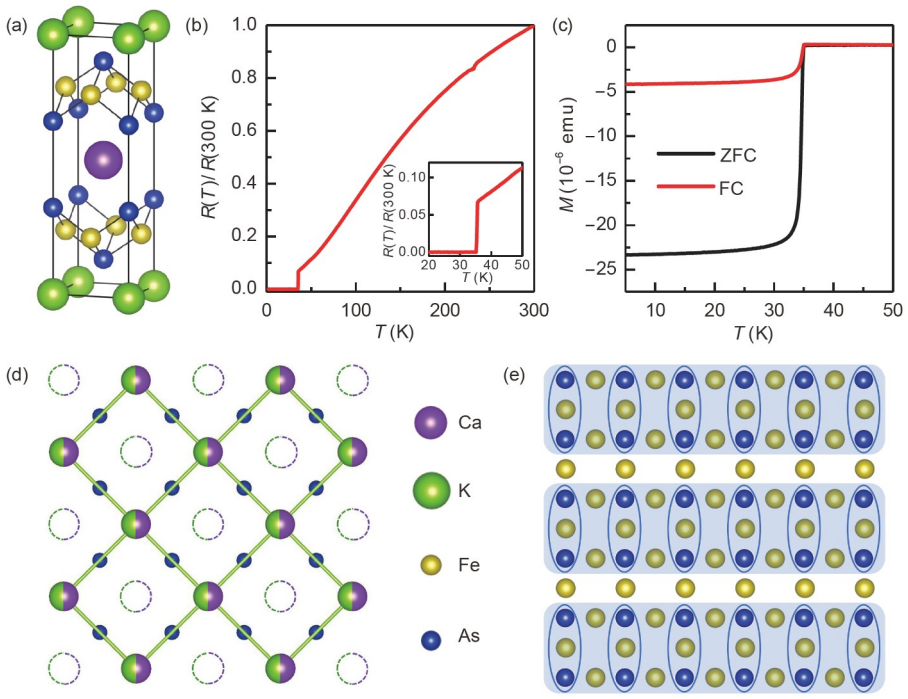

Figure 1 (Color online) (a) Schematic crystal structure of $CaKFe_4As_4$. (b) Temperature dependence of normalized resistance of $CaKFe_4As_4$. Inset: Zoom-in temperature-normalized resistance curve. (c) Temperature dependence of magnetic moments measured in zero-field cooled and field cooled modes with a 10-Oe magnetic field. (d) Schematic illustration of $\sqrt{2} \times \sqrt{2}$ structure formed by AE or A atoms. (e) Schematic illustration of 1×2 stripes (blue stripes) formed by As atoms.

the characteristics of 1×2 reconstructions [7,15]. The morphology in Region-I completely differed from that in Region-II, which indicated that these two regions correspond to different surface terminations. This scenario is further supported by the sharp steps between Region-I and Region-II, as shown by the topological profiles in Figure 2(c) and (d). In some clean areas of Region-I, a square lattice was found. Figure 2(e) depicts a representative image of the square lattice, and the lower inset shows the results of the Fourier transform (FT). According to the FT pattern, the lattice period was calculated to be 5.3 Å, which was approximately $\sqrt{2}$ times the in-plane lattice constant [21]. Therefore, the ordered lattice observed in Region-I resulted from the $\sqrt{2} \times \sqrt{2}$ surface reconstruction.

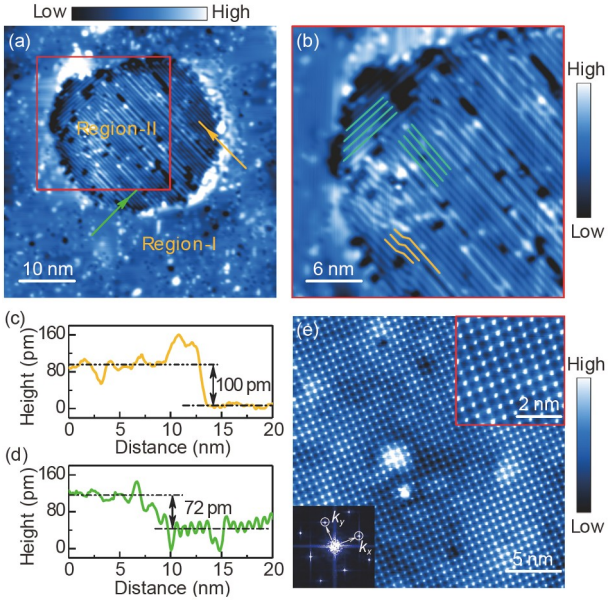

Figure 2 (Color online) (a) STM topographic image (V_{sample}=−40 mV, I_{tip}=100 pA) of $CaKFe_4As_4$. (b) Zoom-in image of the area outlined by the red box in (a). (c), (d) Height profiles taken along the yellow and green arrows in (a), respectively. (e) STM topographic image (V_{sample}=−150 mV, I_{tip}=100 pA) with $\sqrt{2} \times \sqrt{2}$ structure measured in another area of Region-I. The upper inset is a zoom-in image of (e). The lower inset is the FT pattern of (e).

There are several explanations for the origin of surface reconstructions. Since the bonding between the AE/A and As layers was weaker than that in the Fe-As layers, the cleavage was most likely to occur between the adjacent AE/A and As layers, which led to two possible types of exposed surfaces. One was that each side of the cleaved surface acquired 50% AE/A atoms to maintain charge neutrality. In this case, either $\sqrt{2} \times \sqrt{2}$ or 1×2 reconstruction would be induced by the reorder of AE/A atoms due to spontaneous energetic preference [28,36], the surface distortions due to the structural transition from tetragonal to orthorhombic [37], or the inward relaxations of AE/A atoms due to antiferromagnetic ordering [17]. Figure 1(d) shows an example of $\sqrt{2} \times \sqrt{2}$ reconstruction formed by AE/A atoms. The other case was

that the AE/A layer was destroyed, leaving the exposed As layer with some AE/A clusters. The exposed As layer could also form $\sqrt{2} \times \sqrt{2}$ or 1×2 reconstruction due to small buckling that arose in the magnetic orthorhombic phase [36,38,39], the distortions of the Fe layer induced by the structural transition [12], or the relaxations of surface strain due to the underlying AE/A layer [40]. An illustration of 1×2 reconstruction formed by As atoms is shown in Figure 1(e).

Combined with the crystal structure (Figure 1(a)), we argued that the observed $\sqrt{2} \times \sqrt{2}$ and 1×2 lattices corresponded to the reconstructed AE/A and As layers, respectively, because Region-I was 90 pm higher on average than Region-II (see Figure 2(c) and (d) for examples). Nevertheless, it is necessary to clarify why the step height was less than the crystallographic spacing between the AE/A and As layers (150 pm) [21]. In fact, the height recorded by STM depends on both the geometrical corrugations and the local density of states. Therefore, the relatively high density of states in the As layer compared with that in the AE/A layer, supported by theoretical calculations [20], yielded a step smaller than the crystallographic spacing. One may argue that this analysis is not rigorous since the calculated density of states may be further modified by surface reconstructions. Fortunately, in the same layer with Region-I, we captured a new-type morphology with features that reinforced our conclusion. These morphologies shown in Figure 3(a) and (b) not only contain the surface reconstruction highlighted by yellow solid lines but also show a disordered structure, which smoothly merges with the $\sqrt{2} \times \sqrt{2}$ reconstruction. The disordered structure marked by red dots

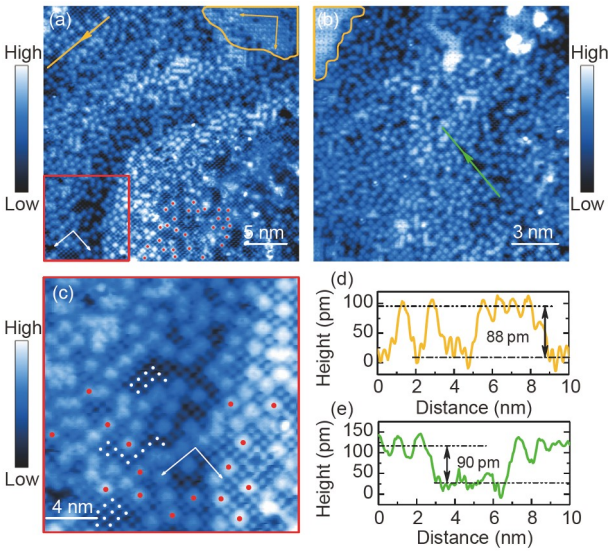

Figure 3 (Color online) (a), (b) Typical STM topographic images of $CaKFe_4As_4$ with surface reconstructions, clusters, and atoms. Setpoint: V_{sample}=−60 mV, I_{tip}=100 pA for (a) and V_{sample}=−100 mV, I_{tip}=100 pA for (b). (c) Zoom-in image of the area outlined by the red box in (a). (d), (e) Height profiles taken along the yellow arrow in (a) and green arrow in (b), respectively.

should be contributed by AE/A atoms that have not yet formed regular lattice after cleavage. The As layer is unlikely to exhibit such a disordered structure because a relatively intact layer is expected due to the strong bonding between As and Fe atoms.

According to our scenario, the As lattice should be observed through the hollows in the AE/A layer. Owing to the covering of AE/A atoms, the underlying As layer might not be reconstructed. As indicated by the white dots in Figure 3(c) (zoom-in image of Figure 3(a)), a lattice with a period of ~3.9 Å was resolved. The period was almost the same as the in-plane lattice constant [21]. This 1×1 lattice was 90 pm lower on average than the $\sqrt{2} \times \sqrt{2}$ lattice (see Figure 3(d) and (e) for examples), reminiscent of the step height between 1×2 and $\sqrt{2} \times \sqrt{2}$ lattices. In addition, the 1×1 lattice was oriented 45° with respect to the $\sqrt{2} \times \sqrt{2}$ lattice (white and yellow coordinate axes), which agreed with the case shown in Figure 1(d). Therefore, it is reasonable to conclude that the 1×1 and 1×2 lattices correspond to the original and reconstructed As layers, respectively, whereas the $\sqrt{2} \times \sqrt{2}$ lattice is contributed by the reconstructed AE/A layer.

Now, we focus on the electronic structures of the As and AE/A layers. Figure 4(b) shows the tunneling spectra collected at several typical locations in Figure 4(a). The tunneling spectrum measured on the intact As layer showed two pairs of peaks located at 7.5 and 18.6 mV. The inner peak is a feature of the superconducting energy gap because the energy value is the same as that reported in other studies [29,38,41,42]. Owing to the large characteristic bias voltage, the origin of the outside peak should be the bosonic mode that is widely observed in iron-based superconductors [43-45]. To reveal this feature more clearly, the second derivative curve d^2I/dV^2 versus V is plotted in Figure 4(d), wherein a clear dip is recognized (black dashed line). Statistically, the energies of the superconducting coherent peak and dip of d^2I/dV^2 were determined to be (7.3±0.4) and (20.0±0.9) mV, respectively. Therefore, the energy value of the bosonic mode was calculated to be $\Omega \approx (20.0-7.3)$ meV=12.7 meV, which agreed with the energy of spin resonance mode measured by inelastic neutron scattering [34,46]. The association between the outside peak and bosonic mode could be further verified by studying the temperature dependence of tunneling spectra in the future [43,47]. The ratio $\Omega/(k_B T_c) \sim$ 4.3 fell into the universal relationship between T_c and the energy of the spin resonance mode [43], indicating the relevance of spin fluctuation in the superconducting pairing of $CaKFe_4As_4$. By contrast, the tunneling spectrum measured on the defect of the As layer (the green dot) did not show a well-defined superconducting gap and bosonic mode, which was likely due to the competition between superconductivity and magnetism induced by the exposed Fe layer [7,48]. Figure 4(c) shows a set of tunneling spectra measured along

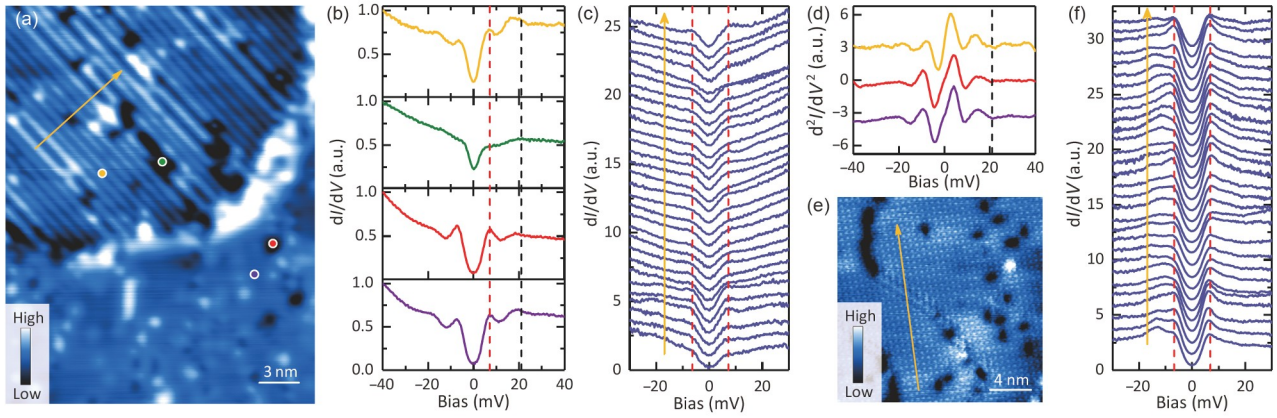

Figure 4 (Color online) (a) STM topographic image (V_{sample}=−60 mV, I_{tip}=100 pA) of $CaKFe_4As_4$. (b) Tunneling spectra measured at the locations marked by the corresponding colored points in (a). The red and black dashed lines indicate the position of the superconducting coherent peaks and the right-wing of the bosonic modes, respectively. (c) Spatially resolved tunneling spectra measured along the yellow arrow in (a). The red dashed lines indicate the position of the superconducting coherent peaks. (d) The second derivative curves calculated from the corresponding colored curves in (b). The black dashed line indicates the location of the dip associated with the bosonic mode. (e) Typical topographic image (V_{sample}=−40 mV, I_{tip}=100 pA) with $\sqrt{2} \times \sqrt{2}$ structure. (f) Spatially resolved tunneling spectra measured along the yellow arrow in (e). The red dashed lines indicate the position of the superconducting coherent peaks.

the yellow arrow in Figure 4(a). Although the differential conductance at high bias voltage varies with position, the energy of the superconducting gap is spatially uniform, indicated by the dashed lines.

As shown by the red and violet curves in Figure 4(b), the tunneling spectra measured on the AE/A layer also have features of the superconducting gap and bosonic mode. Interestingly, the energies of the superconducting gap and bosonic mode (the red and black dashed lines in Figure 4(b)) slightly changed compared with those measured on the As layer, which suggested that the surface reconstructions of $CaKFe_4As_4$ had limited effects on the electronic states. The independence of electronic structures on morphologies was also indicated in another STM study of $CaKFe_4As_4$ [42] and observed in other systems, such as stoichiometric superconductor $KCa_2Fe_4As_4F_2$ [49,50]. There are some reasonable explanations for this phenomenon. (1) The absence of change in the superconducting gap may be induced by the proximity effect since the coherence length of $CaKFe_4As_4$ [51] is larger than the crystallographic spacing between the AE/A and As layers [21]. (2) The density of states of the AE/A layer is featureless despite surface reconstructions. (3) Varied surface terminations mainly affect the spectral weight through the tunneling matrix elements but do not change the pairing strength [8,42]. The homogeneity of electronic states of the AE/A layer was also studied (Figure 4(f)), where the tunneling spectra were measured along the yellow arrow in Figure 4(e). The superconducting gap was found to be relatively homogeneous, which might benefit from the absence of a dopant disorder [6,52].

Finally, we discuss whether the superconducting gap obtained in reconstructed surfaces can represent the bulk properties of $CaKFe_4As_4$. The energies of the superconducting gap measured using bulk-sensitive techniques, such as tunnel-diode resonator [29], polarization-resolved Raman spectroscopy [30], muon spin rotation and relaxation [31], nitrogen-vacancy centers magnetometry [32], and optical conductivity [33], were approximately 5.77, 6.8, 8.6, 8.66, and 9.0 meV, respectively. In our STS experiments, the superconducting gap was determined to be (7.3±0.4) meV, which fell into the range given by bulk-sensitive measurements. In addition, the bosonic mode energy in our experiments agreed with the value obtained by inelastic neutron scattering experiments [34,46]. Therefore, we argue that the electronic states of the surface are similar to those of bulk, regardless of surface reconstructions.

4 Conclusions

In summary, the surface morphologies and electronic states of $CaKFe_4As_4$ were investigated by STM/S. We captured three typical morphologies with 1×1, 1×2, and $\sqrt{2} \times \sqrt{2}$ lattices. By analyzing the geometrical relationships among these morphologies, the 1×1, 1×2, and $\sqrt{2} \times \sqrt{2}$ lattices were identified as the original As, reconstructed As, and reconstructed AE/A layers, respectively. The tunneling spectra collected on the reconstructed As and AE/A layers had an almost identical superconducting energy gap as well as bosonic mode. In addition, the value of the superconducting gap obtained on the reconstructed surface agreed with the value measured using bulk-sensitive techniques. Therefore, the surface reconstructions of $CaKFe_4As_4$ did not significantly change the electronic structure. Our study provides morphological characteristics of various cleavage

surfaces of iron pnictide superconductors and clarifies the limited effects of surface reconstructions on electronic states.

This work was supported by the National Key Basic Research Program of China (Grant Nos. 2017YFA0302902, 2016YFA0300301, 2017YFA0303003, and 2018YFB0704102), the National Natural Science Foundation of China (Grant Nos. 11927808, 11834016, 118115301, 119611410, 11961141008, 11822411, and 11961160699), the Key Research Program of Frontier Sciences, Chinese Academy of Sciences (Grant Nos. QYZDBSSW-SLH008, and QYZDY-SSW-SLH001), the Strategic Priority Research Program (B) of Chinese Academy of Sciences (Grant Nos. XDB25000000, and XDB33000000), the Beijing Natural Science Foundation (Grant Nos. Z190008, and JQ19002), the Key-Area Research and Development Program of Guangdong Province (Grant No. 2020B0101340002), and the CAS Interdisciplinary Innovation Team. H. Luo is grateful for the support from the Youth Innovation Promotion Association of CAS (Grant No. Y202001).

1 Ø. Fischer, M. Kugler, I. Maggio-Aprile, C. Berthod, and C. Renner, Rev. Mod. Phys. **79**, 353 (2007), arXiv: cond-mat/0610672.
2 C. L. Song, and J. E. Hoffman, Curr. Opin. Solid State Mater. Sci. **17**, 39 (2013), arXiv: 1212.5164.
3 A. Yazdani, E. H. da Silva Neto, and P. Aynajian, Annu. Rev. Condens. Matter Phys. **7**, 11 (2016).
4 H. Y. Xue, H. Yang, Y. F. Wu, G. Yao, D. D. Guan, S. Y. Wang, H. Zheng, C. H. Liu, Y. Y. Li, and J. F. Jia, Sci. China-Phys. Mech. Astron. **62**, 76801 (2019).
5 Y. Fei, Y. Zheng, K. L. Bu, W. H. Zhang, Y. Ding, X. J. Zhou, and Y. Yin, Sci. China-Phys. Mech. Astron. **63**, 227411 (2020).
6 C. L. Song, Y. Yin, M. Zech, T. Williams, M. M. Yee, G. F. Chen, J. L. Luo, N. L. Wang, E. W. Hudson, and J. E. Hoffman, Phys. Rev. B **87**, 214519 (2013), arXiv: 1212.3240.
7 A. Li, J. X. Yin, J. Wang, Z. Wu, J. Ma, A. S. Sefat, B. C. Sales, D. G. Mandrus, M. A. McGuire, R. Jin, C. Zhang, P. Dai, B. Lv, C. W. Chu, X. Liang, P. H. Hor, C. S. Ting, and S. H. Pan, Phys. Rev. B **99**, 134520 (2019).
8 J. X. Yin, X. X. Wu, J. Li, Z. Wu, J. H. Wang, C. S. Ting, P. H. Hor, X. J. Liang, C. L. Zhang, P. C. Dai, X. C. Wang, C. Q. Jin, G. F. Chen, J. P. Hu, Z. Q. Wang, A. Li, H. Ding, and S. H. Pan, Phys. Rev. B **102**, 054515 (2020).
9 S. Misra, S. Oh, D. J. Hornbaker, T. DiLuccio, J. N. Eckstein, and A. Yazdani, Phys. Rev. Lett. **89**, 087002 (2002), arXiv: cond-mat/0208053.
10 Y. Zhong, Y. Wang, S. Han, Y. F. Lv, W. L. Wang, D. Zhang, H. Ding, Y. M. Zhang, L. Wang, K. He, R. Zhong, J. A. Schneeloch, G. D. Gu, C. L. Song, X. C. Ma, and Q. K. Xue, Sci. Bull. **61**, 1239 (2016), arXiv: 1607.01852.
11 J. E. Hoffman, Rep. Prog. Phys. **74**, 124513 (2011), arXiv: 1201.1380.
12 V. B. Nascimento, A. Li, D. R. Jayasundara, Y. Xuan, J. O'Neal, S. Pan, T. Y. Chien, B. Hu, X. B. He, G. Li, A. S. Sefat, M. A. McGuire, B. C. Sales, D. Mandrus, M. H. Pan, J. Zhang, R. Jin, and E. W. Plummer, Phys. Rev. Lett. **103**, 076104 (2009), arXiv: 0905.3194.
13 T. Nishizaki, Y. Nakajima, T. Tamegai, and N. Kobayashi, J. Phys. Soc. Jpn. **80**, 014710 (2011).
14 I. Zeljkovic, D. Huang, C. L. Song, B. Lv, C. W. Chu, and J. E. Hoffman, Phys. Rev. B **87**, 201108 (2013), arXiv: 1301.4942.
15 T. M. Chuang, M. P. Allan, J. Lee, Y. Xie, N. Ni, S. L. Bud'ko, G. S. Boebinger, P. C. Canfield, and J. C. Davis, Science **327**, 181 (2010).
16 X. Liu, R. Tao, M. Q. Ren, W. Chen, Q. Yao, T. Wolf, Y. J. Yan, T. Zhang, and D. L. Feng, Nat. Commun. **10**, 1039 (2019).
17 G. Li, L. Liang, Q. Li, M. Pan, V. B. Nascimento, X. He, A. B. Karki, V. Meunier, R. Jin, J. Zhang, and E. W. Plummer, Phys. Rev. Lett. **112**, 077205 (2014).
18 F. Massee, S. de Jong, Y. Huang, J. Kaas, E. van Heumen, J. B. Goedkoop, and M. S. Golden, Phys. Rev. B **80**, 140507 (2009).
19 E. van Heumen, J. Vuorinen, K. Koepernik, F. Massee, Y. Huang, M. Shi, J. Klei, J. Goedkoop, M. Lindroos, J. van den Brink, and M. S. Golden, Phys. Rev. Lett. **106**, 027002 (2011), arXiv: 1009.3493.
20 H. Zhang, J. Dai, Y. Zhang, D. Qu, H. Ji, G. Wu, X. F. Wang, X. H. Chen, B. Wang, C. Zeng, J. Yang, and J. G. Hou, Phys. Rev. B **81**, 104520 (2010), arXiv: 0908.1710.
21 A. Iyo, K. Kawashima, T. Kinjo, T. Nishio, S. Ishida, H. Fujihisa, Y. Gotoh, K. Kihou, H. Eisaki, and Y. Yoshida, J. Am. Chem. Soc. **138**, 3410 (2016).
22 W. R. Meier, T. Kong, S. L. Bud'ko, and P. C. Canfield, Phys. Rev. Mater. **1**, 013401 (2017), arXiv: 1704.09025.
23 M. Rotter, M. Tegel, and D. Johrendt, Phys. Rev. Lett. **101**, 107006 (2008), arXiv: 0805.4630.
24 K. Sasmal, B. Lv, B. Lorenz, A. M. Guloy, F. Chen, Y. Y. Xue, and C. W. Chu, Phys. Rev. Lett. **101**, 107007 (2008).
25 A. S. Sefat, R. Jin, M. A. McGuire, B. C. Sales, D. J. Singh, and D. Mandrus, Phys. Rev. Lett. **101**, 117004 (2008), arXiv: 0807.2237.
26 L. J. Li, Y. K. Luo, Q. B. Wang, H. Chen, Z. Ren, Q. Tao, Y. K. Li, X. Lin, M. He, Z. W. Zhu, G. H. Cao, and Z. A. Xu, New J. Phys. **11**, 025008 (2009), arXiv: 0809.2009.
27 A. Bhattacharyya, D. T. Adroja, M. Smidman, and V. K. Anand, Sci. China-Phys. Mech. Astron. **61**, 127402 (2018), arXiv: 1811.12677.
28 F. Massee, Y. Huang, R. Huisman, S. de Jong, J. B. Goedkoop, and M. S. Golden, Phys. Rev. B **79**, 220517 (2009), arXiv: 0812.4539.
29 K. Cho, A. Fente, S. Teknowijoyo, M. A. Tanatar, K. R. Joshi, N. M. Nusran, T. Kong, W. R. Meier, U. Kaluarachchi, I. Guillamón, H. Suderow, S. L. Bud'ko, P. C. Canfield, and R. Prozorov, Phys. Rev. B **95**, 100502 (2017), arXiv: 1606.06245.
30 W. L. Zhang, W. R. Meier, T. Kong, P. C. Canfield, and G. Blumberg, Phys. Rev. B **98**, 140501 (2018), arXiv: 1804.06963.
31 P. K. Biswas, A. Iyo, Y. Yoshida, H. Eisaki, K. Kawashima, and A. D. Hillier, Phys. Rev. B **95**, 140505 (2017), arXiv: 1704.07578.
32 D. Torsello, K. Cho, K. R. Joshi, S. Ghimire, G. A. Ummarino, N. M. Nusran, M. A. Tanatar, W. R. Meier, M. Xu, S. L. Bud'ko, P. C. Canfield, G. Ghigo, and R. Prozorov, Phys. Rev. B **100**, 094513 (2019), arXiv: 1909.04734.
33 R. Yang, Y. Dai, B. Xu, W. Zhang, Z. Qiu, Q. Sui, C. C. Homes, and X. Qiu, Phys. Rev. B **95**, 140501 (2017).
34 T. Xie, Y. Wei, D. Gong, T. Fennell, U. Stuhr, R. Kajimoto, K. Ikeuchi, S. Li, J. Hu, and H. Luo, Phys. Rev. Lett. **120**, 267003 (2018), arXiv: 1802.01901.
35 G. He, Z. Wei, Z. Feng, X. Yu, B. Zhu, L. Liu, K. Jin, J. Yuan, and Q. Huan, Rev. Sci. Instrum. **91**, 013904 (2020), arXiv: 2003.11296.
36 M. Gao, F. Ma, Z. Y. Lu, and T. Xiang, Phys. Rev. B **81**, 193409 (2010).
37 D. Hsieh, Y. Xia, L. Wray, D. Qian, K. Gomes, A. Yazdani, G. F. Chen, J. L. Luo, N. L. Wang, and M. Z. Hasan, arXiv: 0812.2289.
38 L. Cao, Y. Song, Y. B. Liu, Q. Zheng, G. Y. Han, W. Y. Liu, M. Li, H. Chen, Y. Q. Xing, G. H. Cao, H. Ding, X. Lin, S. X. Du, Y. Y. Zhang, G. Li, Z. Q. Wang, and H. J. Gao, Nano Res. **14**, 3921 (2021).
39 G. Li, X. He, J. Zhang, R. Jin, A. S. Sefat, M. A. McGuire, D. G. Mandrus, B. C. Sales, and E. W. Plummer, Phys. Rev. B **86**, 060512 (2012), arXiv: 1006.5907.
40 F. C. Niestemski, V. B. Nascimento, B. Hu, W. Plummer, J. Gillett, S. Sebastian, Z. Wang, and V. Madhavan, arXiv: 0906.2761.
41 D. Mou, T. Kong, W. R. Meier, F. Lochner, L. L. Wang, Q. Lin, Y. Wu, S. L. Bud'ko, I. Eremin, D. D. Johnson, P. C. Canfield, and A. Kaminski, Phys. Rev. Lett. **117**, 277001 (2016), arXiv: 1606.05643.
42 A. Fente, W. R. Meier, T. Kong, V. G. Kogan, S. L. Bud'ko, P. C. Canfield, I. Guillamón, and H. Suderow, Phys. Rev. B **97**, 134501 (2018).
43 Z. Wang, H. Yang, D. Fang, B. Shen, Q. H. Wang, L. Shan, C. Zhang, P. Dai, and H. H. Wen, Nat. Phys. **9**, 42 (2012), arXiv: 1310.8160.
44 S. Chi, R. Aluru, S. Grothe, A. Kreisel, U. R. Singh, B. M. Andersen, W. N. Hardy, R. Liang, D. A. Bonn, S. A. Burke, and P. Wahl, Nat. Commun. **8**, 15996 (2017), arXiv: 1703.07002.
45 C. Chen, C. Liu, Y. Liu, and J. Wang, Nano Lett. **20**, 2056 (2020).
46 K. Iida, M. Ishikado, Y. Nagai, H. Yoshida, A. D. Christianson, N.

Murai, K. Kawashima, Y. Yoshida, H. Eisaki, and A. Iyo, J. Phys. Soc. Jpn. **86**, 093703 (2017), arXiv: 1708.01006.
47 L. Shan, J. Gong, Y. L. Wang, B. Shen, X. Hou, C. Ren, C. Li, H. Yang, H. H. Wen, S. Li, and P. Dai, Phys. Rev. Lett. **108**, 227002 (2012).
48 A. V. Balatsky, I. Vekhter, and J. X. Zhu, Rev. Mod. Phys. **78**, 373 (2006).
49 X. Chen, W. Duan, X. Fan, W. Hong, K. Chen, H. Yang, S. Li, H. Luo, and H. H. Wen, Phys. Rev. Lett. **126**, 257002 (2021), arXiv: 2102.12150.
50 W. Duan, K. Chen, W. Hong, X. Chen, H. Yang, S. Li, H. Luo, and H. H. Wen, Phys. Rev. B **103**, 214518 (2021), arXiv: 2102.08785.
51 M. Bristow, W. Knafo, P. Reiss, W. Meier, P. C. Canfield, S. J. Blundell, and A. I. Coldea, Phys. Rev. B **101**, 134502 (2020), arXiv: 2003.02888.
52 S. R. Saha, N. P. Butch, T. Drye, J. Magill, S. Ziemak, K. Kirshenbaum, P. Y. Zavalij, J. W. Lynn, and J. Paglione, Phys. Rev. B **85**, 024525 (2012), arXiv: 1105.4798.